

---

This is an electronic reprint of the original article.  
This reprint may differ from the original in pagination and typographic detail.

Jaaranen, Joonas; Fink, Gerhard

## Experimental and numerical investigations of two-way LVL–concrete composite plates with various support conditions

*Published in:*  
Engineering Structures

*DOI:*  
[10.1016/j.engstruct.2022.114019](https://doi.org/10.1016/j.engstruct.2022.114019)

Published: 01/04/2022

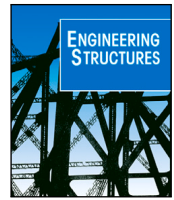
*Document Version*  
Publisher's PDF, also known as Version of record

*Published under the following license:*  
CC BY

*Please cite the original version:*  
Jaaranen, J., & Fink, G. (2022). Experimental and numerical investigations of two-way LVL–concrete composite plates with various support conditions. *Engineering Structures*, 256, Article 114019.  
<https://doi.org/10.1016/j.engstruct.2022.114019>

---

This material is protected by copyright and other intellectual property rights, and duplication or sale of all or part of any of the repository collections is not permitted, except that material may be duplicated by you for your research use or educational purposes in electronic or print form. You must obtain permission for any other use. Electronic or print copies may not be offered, whether for sale or otherwise to anyone who is not an authorised user.



# Experimental and numerical investigations of two-way LVL–concrete composite plates with various support conditions

Joonas Jaaranen<sup>\*</sup>, Gerhard Fink

Department of Civil Engineering, School of Engineering, Aalto University, Espoo, Finland

## ARTICLE INFO

### Keywords:

Timber–concrete  
Two-way plate  
Experimental modal analysis  
Static load test  
Finite element modelling  
LVL

## ABSTRACT

Design of modern timber floors is often governed by the vibration serviceability requirements. One way to improve vibration serviceability is through the design of two-way floor systems. In this paper, the behaviour of two-way LVL–concrete composite plates and a plate strip is investigated experimentally, with an emphasis on the performance of proposed dovetail joint for connecting the adjacent LVL panels. The investigations consist of the experimental modal analysis and static load deformation tests, performed under multiple support conditions. The results show a significant two-way action, indicated by about 45% higher fundamental natural frequency when four edges are supported instead of two. The point load deflection in the centre of the plate was reduced of about 9%. Furthermore, a numerical model for two-way TCC plates was developed and results show a wide agreement with the experimental behaviour, except for discrepancies related to deflections on the plate edge. The results from the experimental and numerical investigations indicate that the dovetail joint can produce a stiff connection, such that the LVL layer could be regarded as continuous in the connected direction.

## 1. Introduction

Design of modern timber floors, especially for longer spans, is often governed by the vibration serviceability requirements, whereas the strength criteria are usually easily fulfilled. The European design standard for timber structures (EN 1995-1-1 [1]) requires vibration serviceability checks for the fundamental natural frequency, static point load deflection and unit impulse velocity response [2]. The acceptable limits are provided in the National Annexes. Fundamentally, the natural frequencies depend on the stiffness-to-mass ratio of the system and the static deflections depend on the stiffness of the system. Therefore, stiffness is an essential parameter for the vibration performance.

Conventional timber floors are inherently one-way system, i.e. the bending stiffness in the lateral direction is small compared to the longitudinal one, and increasing the lateral stiffness can be an effective way to improve vibration serviceability behaviour, e.g. by lateral bracing as discussed in [3]. Another factor relates to the support conditions, such that the vibrational performance can be improved by supporting the floor on all four edges instead of two [4]. The effect, however, also depends on the lateral stiffness of the floor itself.

Over the past few decades, many new timber floor systems, such as cross-laminated timber (CLT) and timber–concrete composite (TCC) floor structures, have emerged. Compared to the conventional joisted or rib-stiffened plate systems, their components have a considerable biaxial load-carrying capacity. For TCCs, this is the case especially

when cross-banded laminated veneer lumber (LVL) or CLT panels are used as the timber layer. However, as the timber layer needs to be assembled from multiple panels due to their limited width, sufficient continuity between them needs to be provided to utilise the biaxial capacity to the full extent. For CLT floors, proposed continuity connection methods include butt-jointing of primed panel edges by 2-components polyurethane glue on-site [5], casting synthetic reaction resin dovetails on-site to precut slots [6] and using splice plates connected to CLT by self-tapping screws [7]. For TCCs, two different connections have been proposed along with the investigations of two-way TCC plates. Loebus et al. [8] investigated two-way CLT–concrete composite plates where the CLT panels were connected by glued-in rebar reinforced joint that was filled with concrete while casting the plate. Although a direct experimental comparison between one-way and two-way plates was not made, the finite element (FE) simulations, with a model based on the experimental results, showed about 40% smaller deflection under a uniform load for a two-way plate compared to a similar one-way plate. Kreis [9] investigated the behaviour of a two-way LVL–concrete composite floor structure with beech LVL, steel tube shear connectors and an intermediate, light-weight insulation layer. The LVL panels' edges were connected by a glued-in rods that were joined together by nuts on-site. The effect of the two-way action was investigated by static load and modal tests with two boundary conditions, two or four edges

<sup>\*</sup> Corresponding author.

E-mail address: [joonas.jaaranen@aalto.fi](mailto:joonas.jaaranen@aalto.fi) (J. Jaaranen).

supported. As a result, activating the two-way action increased the fundamental natural frequency by 43% and decreased deflection under a uniform load (produced by multiple point loads) by 34%. Overall, these two studies showed considerable improvements in stiffness as a result of the two-way action.

Furthermore, the stiffness and strength of the shear connections between timber and concrete are crucial for the performance of TCCs. See e.g. [10–14] for a review of different types of shear connectors. A major difference between one- and two-way TCC systems is that in the one-way systems, the connectors are loaded uniaxially, while in the two-way system, the connectors need to transfer loads in two directions. In [8], inclined screws, aligned according to principal shear flow directions, or notch connections, were suggested for ensuring the adequate performance of the two-way TCC plates.

Uniaxial TCC structures have been widely studied and therefore, also a variety of analysis methods have been proposed. For design purposes, these methods include e.g. the  $\gamma$ -method, the strut-and-tie model and the shear analogy method [12]. For research purposes, a variety of 1D, 2D or 3D FE models that can account for the time-dependent material behaviour or predict the non-linear load response up to the failure, have been presented (see e.g. [10,15,16]). To the authors' knowledge, there are no analytical methods for the mechanical behaviour of the two-way TCC plates, especially with panel-to-panel joints or flexible supports. The numerical models include finite element formulations for layered plates with interlayer slip, e.g. [17,18], but they are not available in common finite element software. Alternatively, each layer can be modelled individually and the interaction between them can be accounted for by contacts or point-wise connections, as was done in [8,9]. In the former, a CLT–concrete plate has been modelled with rigidly connected solid elements and the interlayer slip has been accounted for by adjusting the shear stiffness of the top layer of the CLT. In the latter, the different layers are modelled by shell elements and the layers are coupled by beam elements with the stiffness chosen according to the connection stiffness.

In this paper, an alternative LVL–concrete composite plate, with a new dovetail joint connecting adjacent LVL panels, is introduced. Its potential was shown by experimental and numerical investigations in [19], which, due to the importance of the contact behaviour for the joint, was preceded by the experimental investigations of timber–concrete contacts in [20] and the development of a suitable interface model for simulations in [21]. The shear connection between LVL and concrete is provided by notches, which were chosen due to their biaxial load transfer capability. The choice was further supported by the fact that the notches could be cut with the CNC machine that is anyway needed for efficient manufacturing of the dovetail joint in practice.

The investigations concentrate on the serviceability limit state behaviour: the modal response and static deflection under a concentrated load. The main aims were to investigate performance of the dovetail joint and the effect of the supports conditions, as well as to develop a FE model for predicting the vibration serviceability behaviour of two-way TCC plates. The experimental part consists of testing two large rectangular two-way plates (3.85 x 3.85 m<sup>2</sup>), one with dovetail joints and the other with conventional step joints, with varying support conditions. In addition, a plate strip with the dovetail joints (length 3.85 m) was tested for a focused investigation on the lateral bending behaviour of the connected plate. The tests consisted of experimental modal analysis (EMA) to identify the natural frequencies, damping ratios and mode shapes of the plates, as well as deformation measurements under a concentrated load. Furthermore, a finite model is presented and its predictions are validated against the experimental results.

## 2. Materials and methods

### 2.1. Overview

The experimental investigations included EMA, static deflection tests and destructive tests on three TCC plates. Furthermore, post-test measurements were performed to determine the thickness and

**Table 1**  
Materials used in the experimental investigations.

Plates & material test samples	
LVL	Cross-banded LVL 63 mm (Kerto-Q [22])
Concrete	Self-compacting concrete C30/37 [23], maximum aggregate size 8 mm
Reinforcement	Steel mesh $\phi 4 \times 150 \times 150$ B500A [24]
Concrete grout	Non-shrinking concrete grout C50/60-4 [23], maximum aggregate size 4 mm
Screws	Self-tapping screws 8 $\times$ 80 with flange head, type TBS880 (Rotho Blaas srl, Italy)
Support frames	
LVL	LVL 39 $\times$ 66 (Kerto-T)
GLT	Glued-laminated timber 90 $\times$ 215, GL32c [25]
Screws	Wood screws 6 $\times$ 120, FXA (SwissTech Sourcing Ltd., Vietnam)

density of the concrete layer in the TCC plates, and material tests were conducted to determine the material and interface properties for the FE simulations. The materials used in the experimental investigations are summarised in Table 1 for later references. All the preparations and tests were done in the construction laboratory of Department of Civil Engineering, Aalto University.

### 2.2. TCC plates

The TCC plates comprised a plate strip and two large square plates (two-way plates; Plate 1 and Plate 2). The plates and construction details are illustrated in Fig. 1. All plates consisted of a LVL bottom layer and a top layer of concrete, connected by notch connections with additional screws for uplift. The bottom layers were assembled from three individual LVL panels. The plate dimensions were chosen according to the available space of the testing facilities for the destructive tests. In Plate 1 and the plate strip, the adjacent panels were connected by the novel dovetail joint proposed in [19]. The dovetail joint consisted of pre-cut dovetail patterns and a concrete grout interlayer that was cast after assembly. Detailed illustrations of the dovetail joint are provided in Fig. 2. In Plate 2, a conventional step joint was used and this plate was included as a reference. The main purpose of the plate strip was the investigation of the dovetail joint behaviour under isolated uniaxial bending conditions.

The plates were constructed and tested on the supports illustrated in Fig. 3a for the plate strip and in Fig. 3b for the two-way plates. For stability, the supports for the plate strip were fixed to adjacent walls by horizontal rods, and the supports for the two-way plates were braced by plywood plates fixed to the corners of the frames. During the assembly, additional intermediate supports were used under the joints. Furthermore, the edges of the two-way plates were fixed to the supports by nine, uniformly spaced screws per edge. The plate strip edges were not fixed.

Prior to casting the interlayer, the dovetail joints were treated with a single layer of polyurethane acrylate lacquer, brushed onto the contact surfaces to prevent excessive moisture transfer from the concrete grout to the wood. The concrete layer for the plates was cast two days after the interlayer. After casting, the concrete surfaces were covered with plastic film to prevent evaporation and wetted by spraying water on them once a day for seven days. The intermediate supports were removed prior to testing. All stages of the construction process and the experimental investigation are summarised in Table 2. After the removal of the intermediate supports, the corners of the two-way plates were clearly elevated off from the supports despite being fixed with screws. Also, due to shrinkage, the concrete layer had curled off from the LVL on the edges and corners, and few small cracks were found on the top surface.

The casting and the tests were performed within a 2.5-month period. During the period, in the laboratory, the temperature varied between

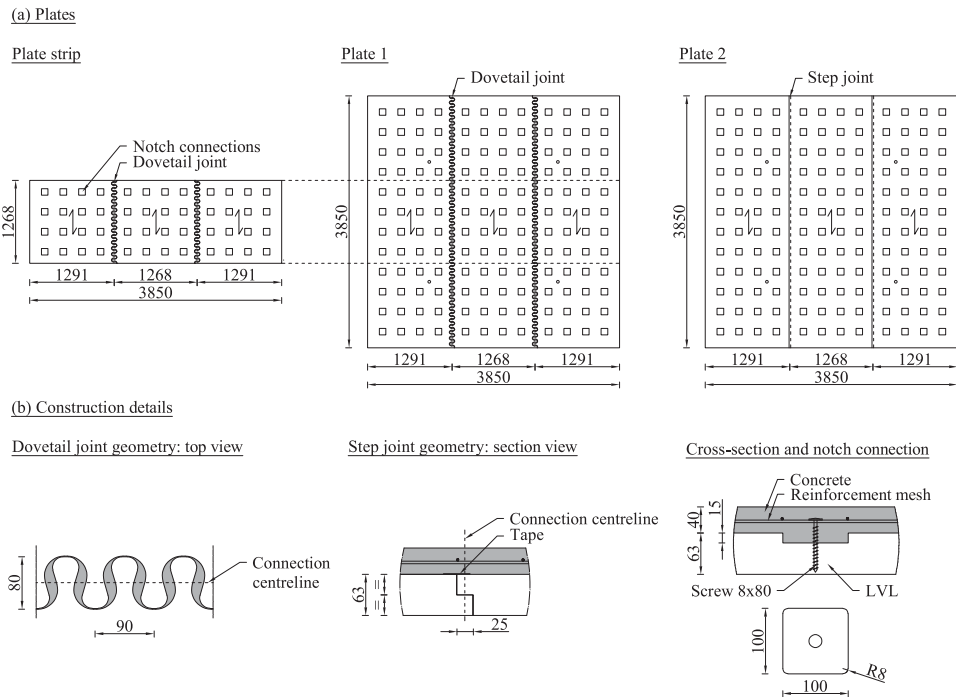


Fig. 1. Geometry of the TCC plates (a) and related construction details (b) with nominal dimensions in [mm].



Fig. 2. Geometry of the dovetail joint with nominal dimensions in [mm] and photos of the joint in Plate 1 before and after casting the interlayer.

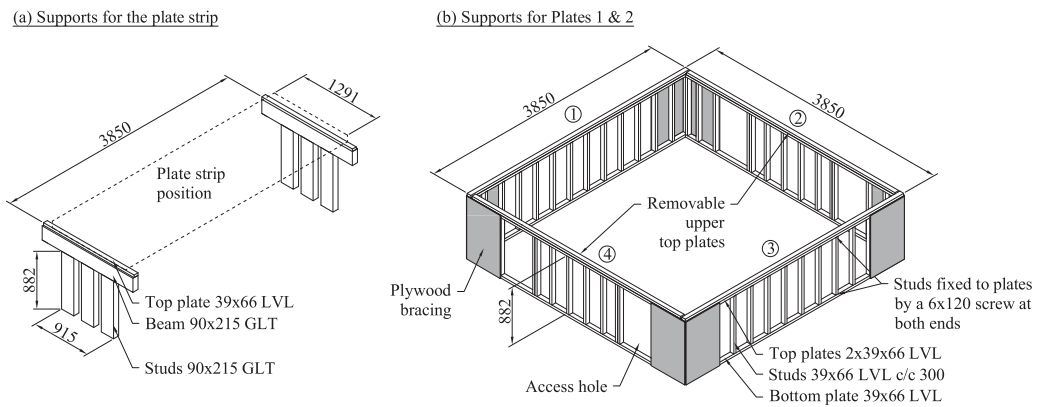


Fig. 3. Structure of the supports for the plate strip and the two-way plates. Dimensions are in [mm].

20 and 22 °C with an average value of 20.6 °C and the relative humidity varied between 13.5 and 31.5% with an average value of 22.6%.

2.3. Non-destructive tests

The non-destructive tests consisted of EMA and static load tests. For the plate strip, the tests were conducted with only one type of support condition, the plate supported on opposite ends (SFSF), as shown in

Fig. 4a. For the two-way plates, the tests were conducted on three different support conditions; all edges supported (SSSS), three edges supported (SSSF), and two opposite edges supported (SFSF), as shown in Fig. 4b. The support conditions were altered by removing the upper top plate of the support.

The EMA was performed using the roving-hammer method [26], in which an accelerometer was fixed in a single location and the plate was impacted at multiple points. The accelerometer was fixed by a

Table 2

Construction and testing stages. The support conditions (SSSS, SSSF, SFSF) are explained in Section 2.3.

Stage	Time from casting
Dovetails joints cast	-2 days
Plates cast	0 days
Curing treatment with water ends	7 days
Plastic sheets removed	14 days
Intermediate supports removed	17 days
Static testing (Plate strip)	18 days
Modal testing (Plate strip)	26 days
Modal testing (SSSS)	26 days
Static testing (SSSS)	33 days
Support 4 removed	33 days
Modal testing (SSSF)	33 days
Static testing (SSSF)	34 days
Support 2 removed	34 days
Static testing (SFSF)	35 days
Modal testing (SFSF)	38 days

magnet on a small steel plate that was glued on the bottom of the TCC plate. Locations for the accelerometer were determined by prior FE simulations, aiming for position where none of the modes had nodal lines (lines with zero amplitude), within the frequency range of interest. Three impacts were performed on each point for averaging. Recorded samples were 4 s long with a frequency of 1024 Hz. All subsequent processing was performed in Matlab [27]. The analysis was limited to frequencies from 5 to 75 Hz, which allowed identification of 6–8 vibration modes that were considered sufficient for the aims of this study. The modal parameters were estimated by Matlab implementation of the least-squares complex exponential (LSCE) method [28]. For the modal parameter estimation, the vibration modes were identified by a stabilisation diagram and subsequent rejection of any mode containing a clearly unphysical mode shape. The identified mode shape vectors were normalised by the method in [29].

The static load tests were performed by placing a mass on the plate and recording the deflection and slip in the chosen locations. In this paper, only the deflections and slips, that were considered the most important, are reported. All the deformations were normalised to a load of 1 kN, which is often used as a criterion for serviceability verification according to EN 1995-1-1 [1]. The normalised deflection and slip, respectively, were calculated by

$$\bar{w} = \frac{w}{m_0 \cdot g} \cdot 1 \text{ kN}, \quad \bar{s} = \frac{s}{m_0 \cdot g} \cdot 1 \text{ kN} \quad (1)$$

where  $w$  and  $s$  are the deflection and slip under the applied mass  $m_0$ , and  $g = 9.81 \text{ m/s}^2$  is the gravitational acceleration. All the values were determined from the deformations of the unloading phase, i.e. removal of the load, assuming it better represents of the elastic stiffness of the system compared to the loading phase. The load was applied for approx. 2.5 min, after which it was removed. The unloading deformation was determined between the moment just before the load removal and 0.5 min after load removal.

The loading positions and measurement points in the static tests are shown in Fig. 4. The plate strip was loaded by a person (71.5 kg) standing on the middle of the plate. The two-way plates were loaded by lifting a weight loaded pallet (0.6 x 0.8 m<sup>2</sup>) onto the plate, as shown in Fig. 5. The pallet had a 30 mm fibre board attached to the bottom to distribute the stresses more evenly.

#### 2.4. Destructive tests and post-test measurements

After the non-destructive tests (Section 2.3), destructive bending tests were also performed on the plate strip (supported on both ends) and the two-way plates (supported on four edges). The results, however, are not presented here since they are not relevant for the serviceability behaviour of the plates. Furthermore, comparison between the

plates was difficult due to variations in the concrete layer thickness and deflection measurement problems encountered during the destructive tests.

After the destructive tests, both two-way plates were demolished by cutting them in three parts and thicknesses of the concrete layers were found to have significant variations. Furthermore, it was suspected that concrete compaction level of the plates was different from compaction level of compression specimens (Section 2.5). Therefore, 36 core samples with a nominal diameter of  $\phi 45 \text{ mm}$  were drilled from the concrete layers of the two-way plates to estimate the thickness and density of the concrete. The thickness measurement was supplemented by measuring the concrete thickness along the cutting lines at every 200 mm.

#### 2.5. Material tests

The material tests consisted of tests on concrete, LVL and the notch connections. For concrete, the compressive strength and modulus of elasticity (MOE) was determined according to Standards [30,31] from cylinders that were cast from the concrete batch used for the plates. The cylinders were cured in the same space with the plates and the tests were conducted at 21, 28 and 77 days age to monitor the development of the strength and stiffness. As an important note, the air content of the concrete, as measured during casting the cylinder specimens, was unusually high, 11.5%.

The tests for LVL consisted of compression and bending tests, parallel and perpendicular to the grain, with specimens cut from the remaining pieces of the panels. The compression tests were used to determine the in-plane compressive MOEs and strengths. The compression tests were performed according to [32] (compression test parallel to the grain), with adapted specimen dimensions ( $b \times l \times h = 63 \times 50 \times 180 \text{ mm}^3$ ). The bending tests were used to determine the bending MOEs and strengths as well as the out-of-plane shear moduli. The bending tests were performed as four-point bending tests as described in [32]. Due to the size limitations of the testing device, the sizes of the specimens were  $b \times h \times l = 50 \times 63 \times 1260 \text{ mm}^3$  with a span of 1.2 m and a distance of 0.4 m between the loading points. The bending MOE and the shear modulus were calculated from the measured global and local deflections between 10% and 40% of the ultimate load. Furthermore, for each LVL specimen, the density and moisture content was determined.

The notch connections were tested by push-out tests with the device described in [14]. The specimens contained a similar notch and were cast from the same concrete batch, as the plates. The tests included two set of specimens: the first set was tested 25 days after casting and the second set was tested 74 days after casting. In the first set, the contact area between LVL and concrete was  $300 \times 450 \text{ mm}^2$ , but due to an unexpectedly strong bond between the concrete and the LVL (in some instances with higher strength than the notch itself), the contact area for the second set was reduced to  $250 \times 350 \text{ mm}^2$  (approximately equal to the area per notch in the plates) by cutting the concrete.

### 3. Experimental results

#### 3.1. Plate strip

In the EMA for the plate strip, seven vibration modes were identified, summarised in Fig. 6. All the modes were clearly distinguished in the experimental frequency response function (FRF). Therefore, it is assumed that all the existing natural frequencies were identified within the range of interest. From the static load tests, normalised point load deformations were  $\bar{w}_1 = 1.45 \text{ mm}$ ,  $\bar{s}_1 = 3.6 \text{ }\mu\text{m}$  and  $\bar{s}_2 = 3.7 \text{ }\mu\text{m}$ , for the mid-point deflection and slips at the ends, respectively.

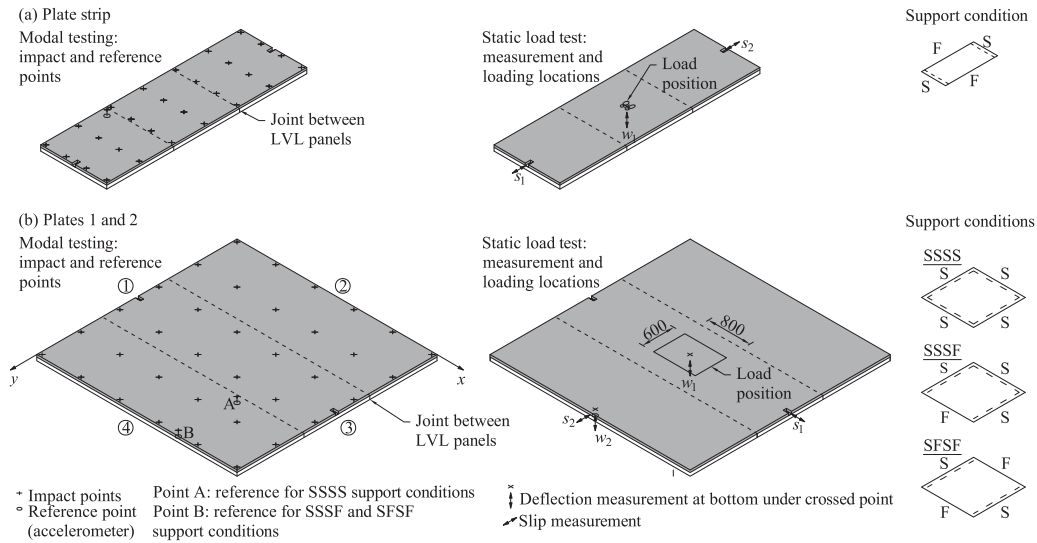


Fig. 4. Impact and reference points for modal testing, measurement and load locations for static testing and support conditions for (a) the plate strip and (b) the two-way plates.

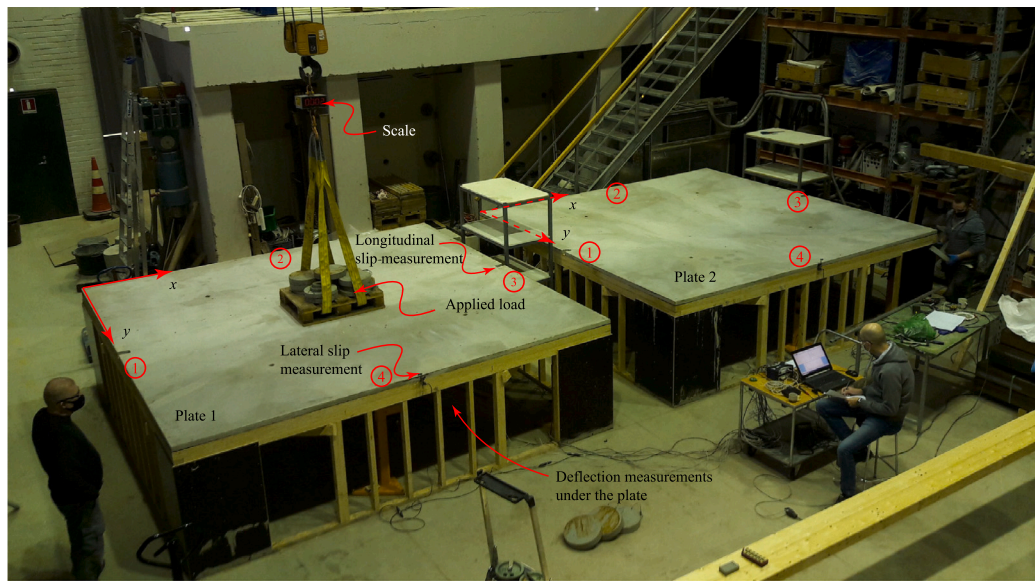


Fig. 5. The two-way plates; static tests as well as general coordinate systems (x, y) and edge numbering (red circles) to help identifying orientation of the plates compared to the other illustrations.

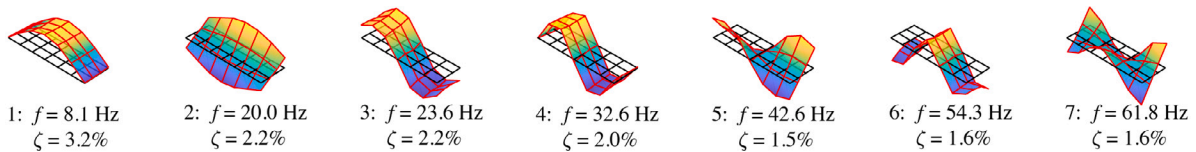


Fig. 6. Experimentally identified modes with corresponding natural frequencies ( $f$ ) and damping ratios ( $\zeta$ ) for the plate strip.

### 3.2. Two-way plates

The results from the EMA and the static tests are summarised in Tables 3 and 4, respectively. The vibration modes were numbered based on the order of appearance. Additionally, in Section 5.2.1, experimental mode shapes and natural frequencies of the four lowest modes are illustrated and compared with the corresponding modes from FE simulations. It has to be noted that there were small resonant peaks in the experimental FRF that were too weak for identification. Furthermore, there were differences between the experimental and identified FRFs

around the resonant frequencies, in some parts of the frequency range. Thus, it is possible that there were additional natural frequencies that could not be identified since the signal was too weak, or they were hidden by other closely spaced modes.

The mean densities for the concrete in Plates 1 and 2 were  $2124 \text{ kg/m}^3$  and  $2113 \text{ kg/m}^3$ , respectively. In these values, only the core samples without visible reinforcements or spacers in them, were considered. These values were considerably higher than the densities of the compression specimens, as suspected.

**Table 3**

Estimated modal parameters (natural frequencies  $f$  and damping ratios  $\zeta$ ) for the two-way plates including average damping ratios and ages at testing for each case.

Mode	SSSS				SSSF				SFSF			
	Plate 1		Plate 2		Plate 1		Plate 2		Plate 1		Plate 2	
	$f$ [Hz]	$\zeta$ [%]										
1	15.7	2.3	15.5	4.2	11.3	2.4	11.1	2.8	10.8	2.5	10.8	2.6
2	29.8	2.5	28.7	5.1	19.2	1.6	19.1	2.0	11.9	2.4	11.9	3.0
3	37.8	3.2	38.1	4.5	31.8	4.1	33.4	3.1	24.0	1.5	25.0	1.6
4	51.1	3.0	43.8	5.5	38.5	2.0	38.3	2.8	31.3	3.7	33.0	2.7
5	53.9	4.1	54.6	2.8	48.2	2.5	49.2	2.6	44.8	3.8	46.3	2.6
6	68.9	1.5	68.4	2.5	55.9	3.3	55.6	4.7	47.9	1.5	48.6	1.3
7	–	–	–	–	67.0	1.4	65.0	2.1	54.5	3.5	56.0	4.0
8	–	–	–	–	–	–	–	–	65.3	1.3	64.7	1.9
Average $\zeta$	2.8		4.1		2.5		2.9		2.5		2.5	
Age <sup>a</sup>	26		26		33		33		38		38	

<sup>a</sup>Age of the concrete during the testing [days].

**Table 4**

Experimental normalised deflections and slips under concentrated load for the two-way plates.

Plate	SSSS		SSSF		SFSF	
	1	2	1	2	1	2
$\bar{w}_1$ [mm]	0.255	0.235	0.266	0.258	0.299	0.278
$\bar{w}_2$ [mm]	0.018	0.019	0.166	0.181	0.158	0.185
$\bar{s}_1$ [ $\mu$ m]	0.97	0.70	0.70	0.58	0.96	0.60
$\bar{s}_2$ [ $\mu$ m]	0.51	0.44	–0.07	0.06	–0.09	0.00

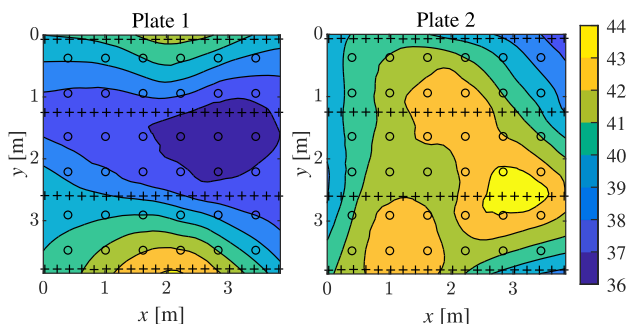


Fig. 7. Concrete thickness [mm] over the two-way plates estimated by fitting to the thickness measurements of drilled core samples (o) and from cut edges (+).

To compare the concrete thickness between the two-way plates, approximate thickness profiles were produced from the local thickness measurements by the curve fitting toolbox available in Matlab [27], using locally weighted regression technique with the ‘lowess’ option. The resulting thickness profiles and the locations for the local measurements are illustrated in Fig. 7. The average thickness of the LVL panels was 64 mm.

### 3.3. Material tests

Results from the material tests are summarised in Table 5. Due to the strong bonding in the LVL–concrete interface, the stiffnesses of the notch connections themselves could not be determined. However, cohesive strength  $\tau_c$  (estimated from the contact area and the slip initiation force), cohesive stiffness  $k_c$  (estimated from the contact area and the initial force–slip stiffness) and ultimate load  $F_u$  (the maximum force after bond failure) are reported here. It should be noted that although the cohesive strength was similar for the different ages, there was a significant increase in the ultimate strength from 25 days to 74 days of age. Potentially, the difference was a result of the LVL drying around the notches, thus leading to a higher compressive strength of the LVL. However, this could not be verified with the existing test data.

### 3.4. Discussion

From the plate strip modal test, it is apparent that the supports possessed significant flexibility, judging by the relatively large amplitudes at the supports. Likely, this had a considerable effect on the natural frequencies of the plate, except for the modes 1 and 4 since they had approximately zero amplitudes at the supports. As a specific detail, the modes 3 and 4 had similar mode shapes, disregarding the amplitudes at supports. However, they are different vibration modes judging by a clear modal separation of 9 Hz. The damping ratios of the plate strip were 1.6–3.3%, agreeing with typical damping ratios for TCCs (about 2.5%) according to [12]. Also, the damping ratios show a clear decreasing trend with increasing mode order.

Considerable support flexibility was also observed in the two-way plate vibration tests. As a result, only the first mode shapes were close to the theoretical mode shapes of simple supported plates. In contrast to the plate strip, the damping ratios vary from mode to mode. The fundamental natural frequencies in the SSSS case were 45% and 44% higher (for Plates 1 and 2, respectively) compared to the SFSF case. The difference is very close to the 43% obtained by Kreis [9], indicating a similar level of two-way action.

By comparison, both two-way plates displayed similar mode shapes (see Section 5.2.1) with small differences between the natural frequencies. The most noteworthy difference is that the SSSS mode 4 for Plate 2 that does not appear for Plate 1. However, this mode had a fairly weak peak in the FRF for Plate 2, and it is possible that a similar mode existed in Plate 1 but was too weak to be identified. Furthermore, comparisons between Plates 1 and 2 identify that the latter had a damping ratio over 1% higher in the SSSS case. However, the difference decreased when the support conditions were changed. In the SFSF cases, both plates have the same damping ratio on average. It is possible that different damping characteristics were caused by the different joints but since only two plates were tested, it was not possible to verify this. In the static tests, the mid-point deflections for Plate 1 were clearly larger than for Plate 2. On the edge, however, opposed to what would be expected, Plate 2 had larger deflections, possibly due to the different support stiffnesses or corner uplift conditions.

Initially, it was expected that Plate 1 would be stiffer compared to Plate 2 due to continuity provided by the dovetail joint. However, the natural frequencies were almost the same and the static mid-point deflections were even smaller in Plate 2. One clear reason for the higher stiffness of Plate 2 was the thicker concrete layer. Another reason might be that the actual stiffnesses of the connections differed from the expected ones. The high stiffness of the dovetail joint was, however, confirmed in the plate strip test. Alternatively, the concrete shrinkage may have pressed the step joint together, creating significant continuity. This phenomenon was therefore adopted to and investigated with the numerical model.

**Table 5**  
Results from the material tests. The values are averages with the coefficient of variation shown in parenthesis ().

Concrete (3+3+3 samples)				
Age [days]	21	28	77	
Density $\rho$ [kg/m <sup>3</sup> ]	2074 (0.02)	2055 (0.02)	2033 (0.00)	
Compressive strength $f_c$ [MPa]	37.2 (0.09)	38.1 (0.04)	39.2 (0.04)	
Initial secant modulus $E_{c,0}$ [GPa]	19.2 (0.09)	20.3 (0.04)	20.4 (0.06)	
Stabilised secant modulus $E_{c,s}$ [GPa]	22.6 (0.08)	22.8 (0.04)	22.4 (0.05)	
LVL compression tests (12+12 samples)				
Grain orientation	Parallel	Perpendicular		
Moisture content [%]	9.8 (0.01)	9.7 (0.02)		
Density $\rho$ [kg/m <sup>3</sup> ]	518 (0.01)	478 (0.01)		
Compressive MOE $E_c$ [MPa]	11246 (0.08)	3018 (0.08)		
Compressive strength $f_c$ [MPa]	39.3 (0.02)	12.2 (0.06)		
LVL bending tests (8+6 samples)				
Grain orientation	Parallel	Perpendicular		
Moisture content [%]	9.8 (0.04)	9.8 (0.02)		
Density $\rho$ [kg/m <sup>3</sup> ]	512 (0.02)	496 (0.04)		
Bending MOE $E_m$ [MPa]	10746 (0.04)	2900 (0.12)		
Shear modulus $G$ [MPa]	116 (0.14)	40 (0.22)		
Bending strength $f_m$ [MPa]	42.9 (0.08)	14.3 (0.19)		
Notch connection tests 25 days age (4+3 samples) and 74 days age (3+3 samples)				
Grain orientation	Parallel	Perpendicular	Parallel	Perpendicular
Age [days]	25	25	74	74
Cohesive stiffness $k_c$ [MPa/mm]	4.90 (0.58)	1.54 (0.65)	3.29 (1.73)	1.21 (0.58)
Cohesive strength $\tau_c$ [MPa]	0.23 (0.16)	0.20 (0.19)	0.23 (0.65)	0.19 (0.19)
Ultimate load $F_u$ [kN]	43.3 (0.05)	29.9 (0.02)	56.1 (0.06)	36.7 (0.04)

Since the plate tests were conducted at different ages, there is an uncertainty related to the concrete properties, especially for the plate strip static tests at the age of 18 days. However, the concrete MOE showed only small differences between the 21–77 days of age and therefore only a small effect is expected.

## 4. Numerical model

### 4.1. General

In this study, a coupled shell approach for modelling the TCC plates was adopted. The simulations were performed in Abaqus [33]. The plates were modelled using 8-node continuum shell elements (SC8R), each part (concrete layer, LVL panels, dovetail joint region) modelled individually. Concrete reinforcement was accounted with two orthogonal rebar layers in the mid-plane of the shell section of the concrete layer, with the nominal rebar diameter and spacing. The varying thickness of the concrete layer was accounted for by adjusting the horizontal positions of the nodes on the top surface of the concrete layer after meshing, according to the measured thicknesses shown in Fig. 7.

The interaction between concrete and LVL parts was accounted for by general contact (general contact definition in Abaqus). The contact was applied uniformly over the whole interface, between concrete and LVL parts, except on a 0.1 m wide region along the plate edges. On the edges, only compressive normal interaction was defined to account for the (observed) curling due to the shrinkage. The connection type between adjacent LVL panels was plate-dependent. For Plate 1 and the plate strip, the dovetail joints were represented by 0.08 m wide dovetail parts. They were modelled by continuum shell elements (SC8R) and connected to the adjacent parts by tie constraints. For Plate 2, the step joints were modelled by the general contact between the adjacent LVL part edges.

Flexibility of the supports had a significant influence on the response of the plates. Therefore, support flexibility was included in the simulation model. The supports were simulated by surface-to-surface contact between support parts (SC8R elements) and the bottom surfaces of the LVL and dovetail joint parts. It should be noted that the purpose of the support part was only to provide a contact surface and aid in visualisations. The model is illustrated in Fig. 8.

Although the contact-based approach for modelling flexible supports may require a larger mesh refinement, it is considerably easier to implement compared to using node-based spring elements, for which the stiffness needs to be defined individually depending on the location and size of the associated elements. Element size  $L/64$  ( $L = 3.85$  m), which was selected based on mesh convergence study, was used for all the modelled parts. The total number of nodes in the models were 74 136 (Plate 1) and 75 580 (Plate 2).

### 4.2. Loads and simulation procedure

Three types of loads were considered in the simulations; self-weight, concentrated static load and concrete shrinkage. The self-weight was applied as a body load. For the static load, load under the pallet was assumed to be shared equally under its long sides (see Fig. 8). The load was applied as uniform pressure over the assumed load distribution area. Shrinkage was included since it has a significant effect on the support conditions, as the shrinkage of the top layer tends to lift the corners and edges up (cupping). Shrinkage strains were simulated with uniform imposed strains over the concrete layer. It is noted that moisture content variations in the LVL might have caused additional deformations but since there was no measured data, this effect was neglected in the model.

The body force for the self-weight was calculated from the defined densities for each material. The pressure for the static load was selected so that the total force is equal to 1 kN. The shrinkage before each step corresponds to the age of the concrete at the following step. The strains were calculated according to fib Model Code 2010 [34] with  $RH = 22.5\%$ , cement type '42.5 N' and drying shrinkage beginning when the plastic films were removed (age of 14 days). The fact that self-compacting concrete was used, was accounted for by multiplying shrinkage strains by 1.2 as suggested in [34].

All plates were analysed by single simulations, in which the self-weight, changes in the support conditions and static loads were introduced incrementally, following the actual order of the construction and testing steps (see Table 2), with an additional shrinkage load step applied before each step. The changes in the support conditions are accounted for by deactivating the supports. All the static load steps were performed as non-linear quasi-static analyses. Furthermore, the natural frequencies were extracted by linear eigenvalue analysis steps

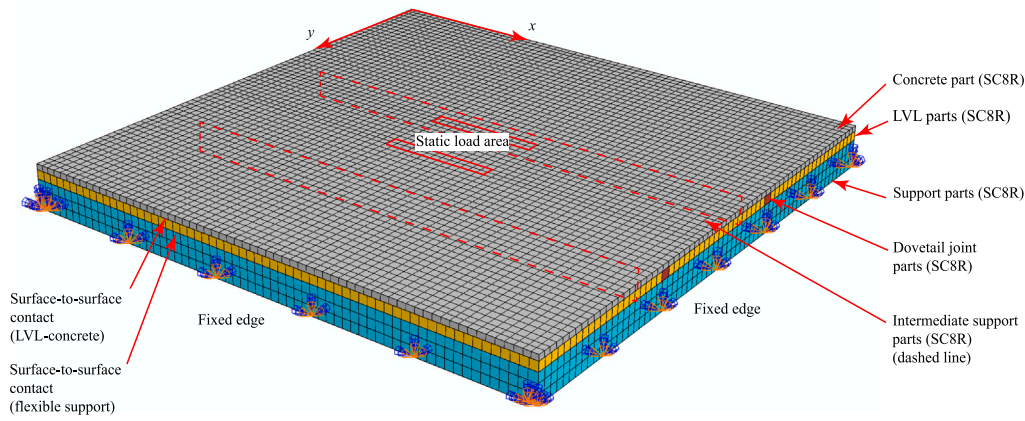


Fig. 8. Finite element model for Plate 1.

included in the simulation according to Table 2. It should be noted that the static loads were not carried on the subsequent steps; the simulation always continued from the base state, prior to applying the static load. Since the node locations do not necessarily coincide with the measurement point locations, interpolation between the nodal values was used to extract the results.

4.3. Constitutive models and parameters

Only low load levels were considered in the simulations. Thus, linearly elastic material models were adopted for all the materials: isotropic for the concrete and steel, and orthotropic for the LVL and dovetail parts. The material properties are summarised in Table 6, where subscripts *x* and *y* refer to directions in Fig. 8 and *z* refers to the out-of-plane direction.

The difference in the measured densities of the concrete (compression test specimens and core samples) indicated that the MOE in the plate was likely higher than the MOE measured in the compression tests. To account for this, the MOE was adjusted according to the difference in the air content, which was about 4%. Based on the regression models presented in [35,36], reduction of the air content by 4% (from 11.5%), for concrete with similar w/c-ratios as in the concrete in this study, leads to increases of about 15% and 21% in the MOE, respectively. The Poisson’s ratio was selected according to the value for the uncracked concrete in [34] and the density was an average from the core sample measurements from Plates 1 and 2. The properties for the LVL were based on the material tests ( $E_x, E_y, G_{xz}, G_{yz}$ ) and manufacturer’s certificate [22] ( $G_{xy}$ ), and the Poisson’s ratio from the previous investigation [19] was used.

Based on the comparison between the experimental and numerical results of the plate strip tests, modelling the dovetail joint with the same elastic properties as the LVL, provides a good agreement. However, simulations with the model presented in [19] indicate a considerably lower stiffness. The discrepancy between the simulation and the experimental observation is likely related to the cohesive stiffness parameters in the simulation. They are the most significant parameters on the joint’s initial stiffness. However, lack of test data prevented validation of the used values. Therefore, the equivalent elastic properties of the dovetail joint were based solely on the Plate Strip tests and were the same as the LVL elastic properties. The density of the dovetail part was calculated based on the geometry of the joint, assuming a density of 2400 kg/m<sup>3</sup> for the concrete grout.

The LVL–concrete interface behaviour was defined by hard contact in compression, and linear cohesive stiffnesses in tension and in shear. The shear stiffnesses were estimated by the cohesive stiffnesses from the notch connection tests (25 days) and adjusted based on comparisons between experimental and predicted slips in the plate strip tests. For the normal stiffness  $k_n$ , a large value was chosen to allow virtually

Table 6  
Material and LVL–concrete interface properties in the FE models.

		Concrete	Steel
Elastic modulus [GPa]	$E$	26.5	200
Poisson’s ratio	$\nu$	0.2	0.3
Density [kg/m <sup>3</sup> ]	$\rho$	2120	7850
		LVL	Dovetail
Elastic moduli [GPa]	$E_x$	11	11
	$E_y$	3	3
Poisson’s ratio	$\nu_{xy}$	0.1	0.1
Shear moduli [GPa]	$G_{xy}$	0.6	0.6
	$G_{xz}$	0.12	0.12
	$G_{yz}$	0.04	0.04
Density [kg/m <sup>3</sup> ]	$\rho$	510	955
		LVL–concrete interface	
Shear stiffnesses [MPa/mm]	$k_{sx}$	5	
	$k_{sy}$	2.25	
Normal stiffness [MPa/mm]	$k_n$	1000	

no separation between the layers. The interface stiffness properties are shown in Table 6.

The axial stiffness of the supports was described by a non-linear force–displacement relation illustrated in Fig. 9a. The quadratic part in compression assumes initial gaps between components, which close gradually with increasing compressive displacement. The linear part accounts for the stage where the gaps have fully closed and the stiffness depends only on the components of the support. In tension, the linear load–displacement response accounts for the uplift stiffness of the whole support assembly, including screws and anchors to the floor.

The load–slip relation was defined by the tensile stiffness  $K_{N,t}$ , initial gap  $u_0$  (defining the size of the quadratic part) and compressive stiffness  $K_{N,c}$  (slope of the linear part in compression). For the initial gap,  $u_0 = 0.5$  mm was assumed. The compressive stiffness was estimated as  $K_{N,c} = 20$  kN/mm/m, based on an approximate analytical model, where axial stiffness at each stud was estimated by a series of springs (bottom plate, stud and two top plates) and smeared over a unit length by dividing by the stud spacing. The spring stiffnesses for the top and bottom plates were estimated assuming that stresses spread out at a 45° angle. Furthermore, the nominal dimensions and the mean MOE of the LVL (Kerto-T) parallel to the grain and perpendicular to grain (flatwise) were used in the calculation. Due to the highly complex load transfer mechanism in tension, the tensile stiffness could not be reliably calculated so it was roughly approximated as  $K_{N,t} = 1/8 K_{N,c} = 2.5$  kN/mm/m.

Horizontal stiffness of the support was assumed to have a negligible effect on the plate behaviour. However, to prevent rigid body motions, small shear stiffnesses were defined. Since the supports were presented by area contacts, the stress–displacement relations for the model were

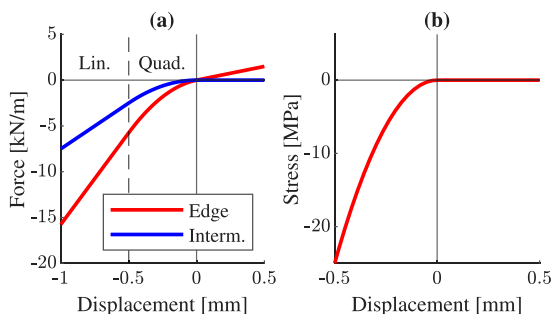


Fig. 9. Defined load–displacement relations for (a) the edge and the intermediate supports and (b) the contact between the panel edges for Plate 2.

obtained by dividing the force by the width of the contact area. For the intermediate supports, stud spacing was twice the spacing of the edge supports. Thus, the intermediate supports were assumed to have half the compressive stiffness of the edge supports and no tensile stiffness, as the plate was not fixed to the intermediate supports.

The contact between the panels (Plate 2) was defined by compressive normal behaviour: if the contact separates, no stresses are transferred, if the contact closes, the normal stresses are defined by a quadratic stress–displacement relation shown in Fig. 9b.

The simulations were performed on a standard desktop computer (2.10 GHz CPU, 16 GB RAM), resulting in computation times of 31 min (Plate 1) and 35 min (Plate 2). The long computation times resulted from the large number load steps and non-linearities caused by the contacts and deactivation of supports.

#### 4.4. Adjustments for the plate strip

The plate strip tests were simulated with a similar model as the two-way plates, except that the dimensions of the plate were adapted, support conditions covered only the SFSF case and the static load was applied on a 0.1x0.1 m<sup>2</sup> area in the centre of the plate. The compressive stiffness of the supports was also adapted, based on the different material and geometry of the supports. Using a similar analytical approximation as for the two-way plates (see Section 4.3), yielded a compressive stiffness of  $K_{N,c} = 75$  kN/mm/m. The initial gap was assumed the same as for the other supports ( $u_0 = 0.5$  mm) and tensile stiffness was set to zero since no screws were used. The plate strip model had 27 882 nodes in total and the computation time was 4.5 min.

### 5. Model results

#### 5.1. Plate strip

Comparisons between the experimental and numerical deflection, slip and fundamental frequency are presented in Table 7, and a detailed comparison of the natural frequencies and mode shapes are shown in Fig. 10. The vibration modes were predicted between 7 and 70 Hz. There is a good agreement between the experimental and numerical results with less than 10% prediction error, however, stiffness is fairly underestimated. With respect to modal analysis, it should be noted that while most modes have similar shapes and the natural frequencies are consistent with the experimental results, the model predicts only a single S-shaped mode (mode 3), instead of two separate experimental S-shaped bending modes (mode 3 and 4).

Table 7

Comparison of experimental and numerical results for the plate strip tests. Err% is the relative error of the numerical prediction in [%].

	Experimental	Numerical	Err%
$\bar{w}$ [mm]	1.45	1.50	3.4
$\bar{s}$ [μm]	3.65 <sup>a</sup>	3.3	-6.3
$f_1$ [Hz]	8.1	7.7	-4.9

<sup>a</sup>Average from the two ends.

#### 5.2. Two-way plates

##### 5.2.1. Modal analysis

The model was used to predict the vibration modes with natural frequencies from 10 to 70 Hz for each case, which was a large enough range to find all the similar modes, as obtained from the experimental investigations. Accuracy of the predictions was evaluated in two steps. First, the experimental modes were matched to the corresponding numerical modes by correlations between the mode shapes, and second, the natural frequencies of the matched modes were compared. The mode matching was performed by calculating Model Assurance Criterion (MAC) [26] between all the numerical and experimental modes, and for each experimental mode, the matching numerical mode was the one with the highest MAC value. The MAC value for a pair of modes is calculated by

$$MAC_{i,j} = \frac{|\phi_i^T \phi_j|^2}{(\phi_i^T \phi_i)(\phi_j^T \phi_j)} \quad (2)$$

where  $\phi_i$  is the mode shape vector for numerical mode  $i$  and  $\phi_j$  is the mode shape vector for experimental mode  $j$ . However, there existed also numerical modes that did not appear in the experimental results. Furthermore, while most of the modes could be easily matched, there were particular experimental modes that had almost the same MAC with two adjacent numerical modes. These modes also had lower MAC values compared to other matching modes. Fig. 11 shows the four lowest numerical modes, plotted against the matched experimental modes and Fig. 12 shows the natural frequencies of all the experimentally identified modes compared to the natural frequencies of the matching numerical modes.

##### 5.2.2. Static load deflection

Comparisons of the experimental and numerical normalised deformations are shown in Table 8. The comparisons include only the deflections since it is usually the measure of interest regarding serviceability. Predictions related to the mid-point deflections were fairly accurate. However, deflections on the edge of the plates were less accurate, especially for Plate 2. This discrepancy is further discussed in Section 5.3.

#### 5.3. Discussion

The model predictions had a wide agreement with the experimental data. The model was able to predict the natural frequencies with correct mode shapes although small deviations existed. Also, the static load deflections at the loaded location, were predicted within approx. ±5% error. The largest differences were related to the static load deflections on the edge of the two-way plates. For Plate 1, the deflections were underestimated by 10–12.5%, and for Plate 2, they were underestimated up to 30.4%. While the differences related to Plate 1 could have been potentially caused by e.g. variation of stiffness between LVL panels, the differences related to Plate 2 were too large to be explained by the variation of the material properties. Multiple effects, e.g. varying LVL stiffness, different step joint compressive stiffnesses and different interlayer stiffnesses, were tested with simulations, but none of them could explain the observed difference between the experiment and the

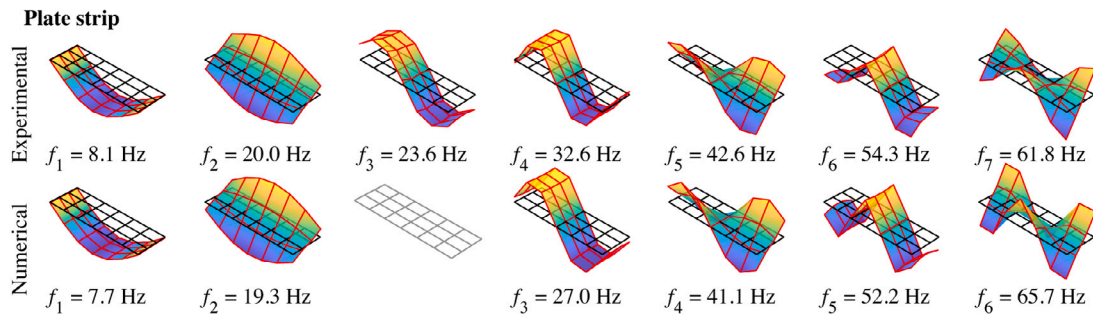


Fig. 10. Comparison of experimentally identified and numerical mode shapes for the plate strip. Numerical modes have been aligned with the experimental modes by matching the mode shapes.

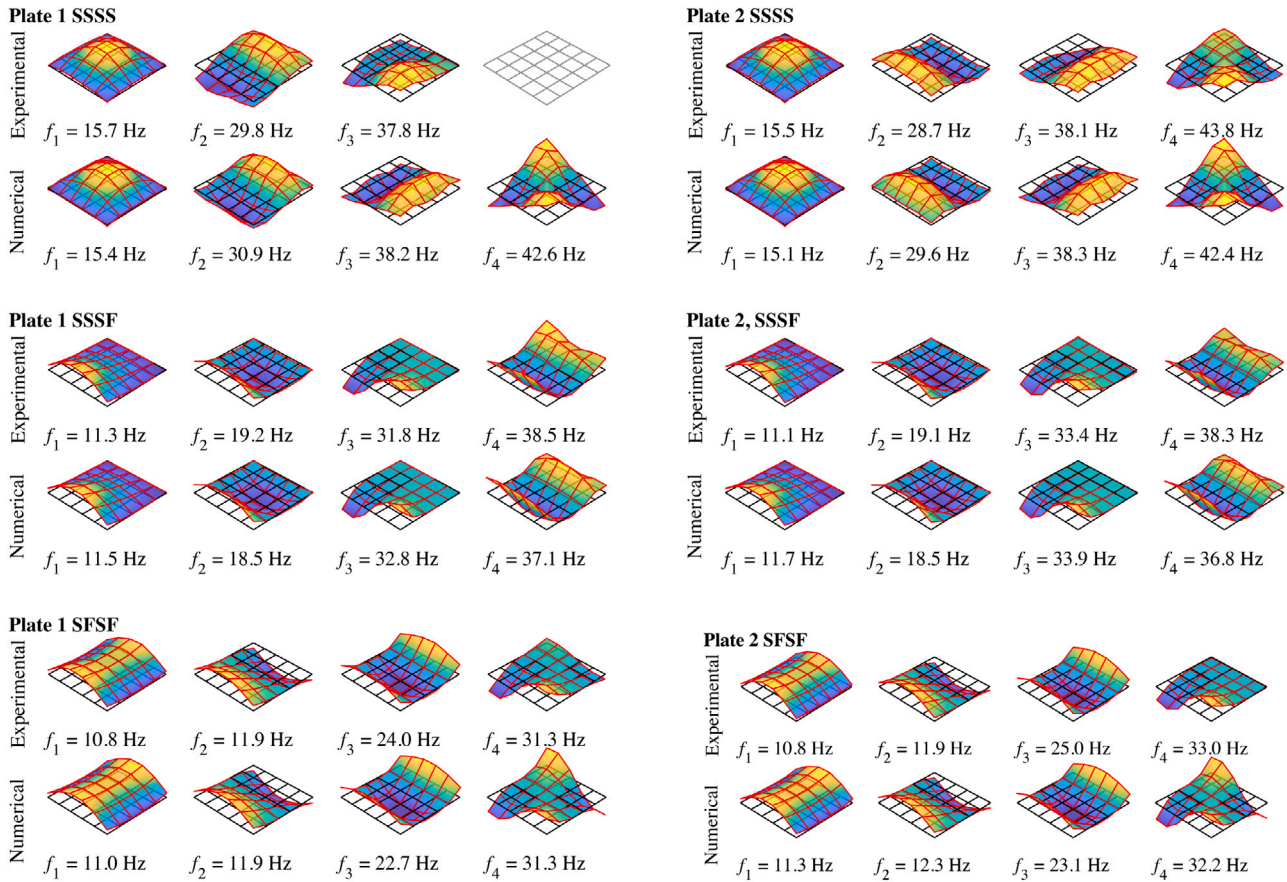


Fig. 11. Comparison of four lowest, matched experimental and numerical modes for the two-way plates.

Table 8

Experimental and numerical normalised deflections for the two-way plates. Err% is the relative error of the numerical prediction in [%].

		SSSS			SSSF			SFSSF		
		Exp.	Num.	Err%	Exp.	Num.	Err%	Exp.	Num.	Err%
Plate 1	$\bar{w}_1$ [mm]	0.255	0.262	2.7	0.266	0.281	5.5	0.299	0.298	-0.4
	$\bar{w}_2$ [mm]	0.018	0.016	-12.3	0.166	0.148	-10.5	0.158	0.138	-12.5
Plate 2	$\bar{w}_1$ [mm]	0.235	0.246	4.5	0.258	0.257	-0.7	0.278	0.268	-3.6
	$\bar{w}_2$ [mm]	0.019	0.015	-24.0	0.181	0.133	-26.3	0.185	0.129	-30.4

simulation. It is likely that the differences were caused by the effects that were not accounted for in the model, such as varying support stiffness, different curling pattern due to shrinkage, or effects of creep. However, as mentioned in Section 3.4, Plate 2 had an unexpectedly large edge deflection compared to Plate 1 and a clear reason could not be pointed out. Further validations are needed to find whether this

particular discrepancy was caused by the model or inaccuracies in the test setup.

The comparison between the plate strip tests and simulation suggest that the dovetail joint provides a stiffness that is similar to the stiffness of an intact panel. However, it has to be noted that, only one single strip was tested. The finding is supported also by the simulations for

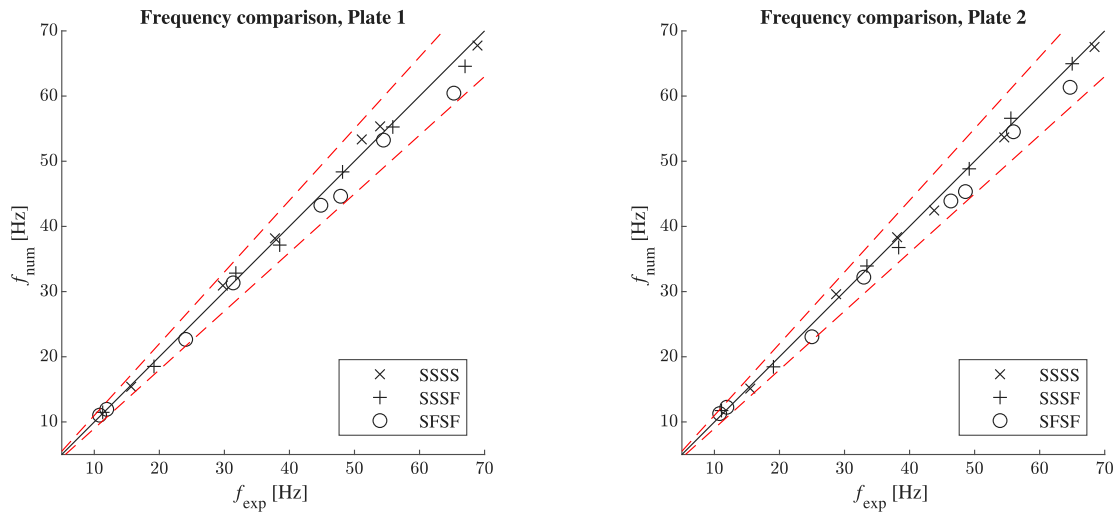


Fig. 12. Comparison of the natural frequencies between experimental modes and matched numerical modes for the two-way plates. The black line represent equal natural frequencies and the dashed red lines represent  $\pm 10\%$  prediction error bounds.

Plate 1, where the assumed stiffness provided a good agreement with the experimental data.

In the model for Plate 2, it was assumed that the joint transfers axial stresses under compression (which is caused by concrete shrinkage). Validity of this assumption was tested by an additional simulation with a zero compressive stiffness assigned to the step joints. Compared to the base case (compressive stiffness accounted for), the prediction errors were significantly larger. Maximum error in natural frequencies was over 21% and deflections due static loads were larger in the centre (up to 11% error) and lower on the edges (up to 43% error). This shows that continuity induced by the joint being pressed together by shrinkage is a plausible explanation (together with the larger thickness of the concrete layer) for the unexpectedly small difference between Plates 1 and 2. However, even if this shrinkage-induced compression between adjacent panels is able to provide lateral continuity, it can hardly be considered as a reliable load transfer mechanism over the service life that could be applied in the practical design of TCC floors. Still, the phenomenon should be further investigated for better understanding.

A noteworthy difference between the experiments and model predictions was that not all predicted vibration modes appeared in the experimental results. However, based on the simulations, in a large portion of the numerical mode shapes that did not appear in the experimental results, the reference (accelerometer) location is very close to the nodal line (lines with a zero amplitude) of the predicted mode shapes. In total, in 10 out of 14 non-matched numerical modes, the reference point was close to or directly at the nodal line. Based on this, it is possible that many of the modes that could not be matched, existed in the experimental plates but could not be identified due to too low accelerations at the reference location. Alternatively, it is possible that the model could not produce all of the modes of the real structure due to inaccuracies or simplifications. However, validating this was not possible with the existing data. In the planned follow-up studies, multiple accelerometers will be used to avoid potential problems with the placement. In addition, the early simulations used to select the reference locations did not account for the support flexibility, leading to inaccurate predictions of the mode shapes and therefore, a suboptimal placement of the reference points. With the refined model, uncertainty related to the effective placement of the accelerometers can be reduced.

## 6. Conclusion

In this paper, experimental and numerical investigations of two-way LVL-concrete composite plates are presented. The experimental investigations included modal tests and static load testing of two two-way

plates with different connections between the LVL panels; a dovetail joint and a conventional step joint. Also, a one-way plate strip with the dovetail joint was investigated. The main aims of the study were to investigate the overall vibration behaviour of a two-way plate with the dovetail joint (providing lateral continuity between individual LVL panels) and the effects of different support conditions. The plate with the step joint was included as a reference, and the plate strip for investigating the joint's behaviour under uniaxial bending conditions. Furthermore, a numerical model for the plates, including flexible supports and concrete shrinkage effects, is presented and validated, showing a wide agreement with the experimental results. The model is able to predict the natural frequencies and point load deflections at the loaded position with less than 10% errors and predict correct mode shapes. However, there are differences related to the predicted modes and larger errors in the deflections on the edge of plate.

Based on the experimental results and numerical simulations, panels that are connected with the dovetail joint have a stiffness similar to a continuous panel. The experimental results showed a significant increase of the plate stiffness with two-way conditions compared to one-way conditions; with the measured natural frequencies being about 45% higher, which agrees also with other related studies. The point load deflection at the centre of the plate decreased by about 9% with the two-way conditions.

Although a significantly higher stiffness was expected from the plate with the dovetail joint compared to the reference plate, the results are very similar for both plates. Partly, this discrepancy was explained by the significantly thicker concrete layer in the reference plate due to construction tolerances. However, the step joint can potentially provide significant continuity between LVL panels due to pre-stress caused by the concrete shrinkage pressing joint surfaces together. This assumption was validated by numerical comparison, but further investigations are needed on the topic and the effect could hardly be considered a reliable method of providing continuity between panels in design.

The results show a clear potential for improving the vibration behaviour by designing the floors as two-way TCC systems. However, the number of the experiments was limited and the plates had shorter spans than a typical TCC floor plate. The presented model, however, is considered theoretically valid for any span, as long as the plate is thin or moderately thick. Furthermore, the model showed a good agreement with the experiments and is therefore considered suitable for studying the effects of different spans, cross-sections and connections for two-way TCC plates. It is clear though that the accuracy of the model should be validated also for longer spans. The study shows also an important issue related to the modelling of plates on flexible supports: if the

supports exhibit significant flexibility and/or the uplift can occur in the corners, the vibration modes can be significantly different from the theoretical modes for simply supported plates. Therefore, it is essential to identify the mode shapes and perform mode matching for the model validation in those cases.

### CRedit authorship contribution statement

**Joonas Jaaranen:** Conceptualization, Writing – original draft, Writing – review and editing, Methodology, Investigations, Formal analysis, Software, Visualization, Project administration. **Gerhard Fink:** Conceptualization, Writing – review and editing, Project administration, Funding acquisition.

### Declaration of competing interest

The authors declare that they have no known competing financial interests or personal relationships that could have appeared to influence the work reported in this paper.

### References

- [1] SFS-EN 1995-1-1, Eurocode 5: Design of timber structures - Part 1-1: General - common rules and rules for buildings, standard. Helsinki: Finnish Standards Association; 2004.
- [2] Zhang B, Rasmussen B, Jorissen A, Harte A. Comparison of vibrational comfort assessment criteria for design of timber floors among the European countries. *Eng Struct* 2013;52:592–607. <http://dx.doi.org/10.1016/j.engstruct.2013.03.028>.
- [3] Weckendorf J, Toratti T, Smith I, Tannert T. Vibration serviceability performance of timber floors. *Eur J Wood Wood Prod* 2015;74(3):353–67. <http://dx.doi.org/10.1007/s00107-015-0976-z>.
- [4] Smith I. Vibrations of timber floors: Serviceability aspects. In: Thelandersson S, Larsen HJ, editors. *Timber engineering*. West Sussex: Wiley; 2003, p. 241–66.
- [5] Zöllig S, Frangi A, Franke S, Muster M. Timber structures 3.0 - new technology for multiaxial slim, high performance timber structures. In: *Proceedings of WCTE, World Conference on Timber Engineering*. Vienna, Austria; 2016.
- [6] Maurer B, Maderebner R, Zingerle P, Färberböck I, Flach M. Point-supported flat slabs with clt-panels. In: *WTCE, World Conference on Timber Engineering*. Seoul, Republic of Korea; 2018.
- [7] Asselstine J, Lam F, Zhang C. New edge connection technology for cross laminated timber (CLT) floor slabs promoting two-way action. *Eng Struct* 2021;233:111777. <http://dx.doi.org/10.1016/j.engstruct.2020.111777>.
- [8] Loebus S, Dietsch P, Winter S. Two-way spanning CLT-concrete-composite-slabs. In: *Proceedings of INTER - International Network on Timber Engineering Research*. Kyoto, Japan; 2017.
- [9] Kreis B. Two-way spanning timber-concrete composite slabs made of beech laminated veneer lumber with steel tube connection (Phd Thesis), ETH Zürich; 2021.
- [10] Yeoh D, Fragiaco M, Franceschi MD, Boon KH. State of the art on timber-concrete composite structures: Literature review. *J Struct Eng* 2011;137(10):1085–95. [http://dx.doi.org/10.1061/\(asce\)st.1943-541x.0000353](http://dx.doi.org/10.1061/(asce)st.1943-541x.0000353).
- [11] Dias AMPG. Analysis of the nonlinear behavior of timber-concrete connections. *J Struct Eng* 2012;138(9):1128–37. [http://dx.doi.org/10.1061/\(asce\)st.1943-541x.0000523](http://dx.doi.org/10.1061/(asce)st.1943-541x.0000523).
- [12] Dias A, Schänzlin J, Dietsch P, editors. *A state-of-the-art report by COST action FP1402 / WG. Vol. 4*. Shaker Verlag; 2018.
- [13] Di Nino S, Gregori A, Fragiaco M. Experimental and numerical investigations on timber-concrete connections with inclined screws. *Eng Struct* 2020;209:109993. <http://dx.doi.org/10.1016/j.engstruct.2019.109993>.
- [14] Derikvand M, Fink G. Deconstructable connector for TCC floors using self-tapping screws. *J Build Eng* 2021;42:102495. <http://dx.doi.org/10.1016/j.jobe.2021.102495>.
- [15] Khorsandnia N, Schänzlin J, Valipour H, Crews K. Coupled finite element-finite difference formulation for long-term analysis of timber-concrete composite structures. *Eng Struct* 2015;96:139–52. <http://dx.doi.org/10.1016/j.engstruct.2015.03.047>.
- [16] Khorsandnia N, Valipour H, Bradford M. Deconstructable timber-concrete composite beams with panelised slabs: Finite element analysis. *Constr Build Mater* 2018;163:798–811. <http://dx.doi.org/10.1016/j.conbuildmat.2017.12.169>.
- [17] Thompson EG, Vanderbilt M, Goodman J. FEAFLO: A program for the analysis of layered wood systems. *Comput Struct* 1977;7(2):237–48. [http://dx.doi.org/10.1016/0045-7949\(77\)90042-6](http://dx.doi.org/10.1016/0045-7949(77)90042-6).
- [18] Latham CT, Toledano A, Murakami H, Seible F. A shear-deformable two-layer plate element with interlayer slip. *Internat J Numer Methods Engrg* 1988;26(8):1769–89. <http://dx.doi.org/10.1002/nme.1620260807>.
- [19] Jaaranen J, Fink G. Experimental and numerical investigations of a timber-concrete dovetail splice joint. *J Build Eng* 2021;43:103179. <http://dx.doi.org/10.1016/j.jobe.2021.103179>.
- [20] Jaaranen J, Fink G. Frictional behaviour of timber-concrete contact pairs. *Constr Build Mater* 2020;243:118273. <http://dx.doi.org/10.1016/j.conbuildmat.2020.118273>.
- [21] Jaaranen J, Fink G. Cohesive-frictional interface model for timber-concrete contacts. *Int J Solids Struct* 2021;111174. <http://dx.doi.org/10.1016/j.ijsolstr.2021.111174>.
- [22] Eurofins expert services Oy, EUFI29-20000676-C/E: Product certificate, Kerto-S and Kerto-Q, structural laminated veneer lumber. Updated December 22, 2020.
- [23] SFS-EN 206:2014+A1:2016: Concrete. Specification, performance, production and conformity, standard. Helsinki: Finnish Standards Association; 2016.
- [24] SFS-EN 1300:2020: Reinforcing steels. Minimum requirement for weldable reinforcing steels and welded fabrics, standard. Helsinki: Finnish Standards Association; 2020.
- [25] SFS-EN 14080: Timber structures. Glued laminated timber and glued solid timber. Requirements, standard. Helsinki: Finnish Standards Association; 2013.
- [26] Ewins D. *Modal testing: theory, practice and application*. second ed.. Wiley; 2009.
- [27] The Mathworks Inc. MATLAB. version 9.9.0.1495850 (R2020b). Natick, Massachusetts; 2020.
- [28] Brown DL, Allemang RJ, Zimmerman R, Mergeay M. Parameter estimation techniques for modal analysis. SAE technical paper series, SAE International; 1979. <http://dx.doi.org/10.4271/790221>.
- [29] Phillips A, Allemang R. *Topics in modal analysis II*, Vol. 8. Springer; 2014, p. 29–41, Ch. Normalization of Experimental Modal Vectors to Remove Modal Vector Contamination.
- [30] SFS-EN 12390-3: Testing hardened concrete. Part 3: Compressive strength of test specimens, standard. Helsinki: Finnish Standards Association; 2019.
- [31] SFS-EN 12390-13: Testing hardened concrete. Part 13: Determination of secant modulus of elasticity in compression, standard. Helsinki: Finnish Standards Association; 2014.
- [32] SFS-EN 408 A1: Timber structures. Structural timber and glued laminated timber. Determination of some physical and mechanical properties, standard. Helsinki: Finnish Standards Association; 2012.
- [33] Dassault systèmes. Abaqus 2018 documentation. Providence, USA; 2017.
- [34] Walraven J, van der Horst A. FIB model code for concrete structures 2010, FIB. 2013.
- [35] Klaiber FW, Thomas TL, Lee DY. Final report: fatigue behavior of air-entrained concrete - phase II. Resreport, Iowa State University, Engineering Research Institute; 1979.
- [36] Lee DY, Klaiber FW, Coleman JW. Final report: fatigue behavior of air-entrained concrete. resreport, Iowa State University, Engineering Research Institute; 1977.